Fusion Framework for Coaxial Catheter Tracking

Xuan Thao Ha, Di Wu, Fabian Trauzettel, Mouloud Ourak, Gianni Borghesan, Arianna Menciassi, and Emmanuel Vander Poorten

***Abstract*— Minimally invasive catheter-based interventions normally take place under the guidance of fluoroscopy. However, fluoroscopy is harmful to both patients and clinicians. Moreover, it only offers 2D shape visualization of flexible devices. To solve the problem of harmful radiation and offer 3D pose and shape information, recent studies propose a combination of Electromagnetic Tracking (EMT) sensors and multi-core Fiber Bragg Grating (FBG) fiber sensing. However, for robust localization, at least two EMT sensors are required to be attached to each multi-core fiber. This may make the catheter overly complex and fragile. Furthermore, the inability of multi-core FBG fibers to distinguish between twist-induced strain and bend-induced strain impacts shape sensing accuracy. This paper proposes a new approach offering a precise shape sensing method that is robust against torsional twists and exploits symmetry and geometry to compensate for limited sensing information. The proposed approach originates from the observation that many interventional procedures employ a plurality of concentric instruments. By distributing sensors over these instruments, the complexity per instrument can be kept acceptable. The proposed sensor fusion approach ensures robust and superior shape reconstruction. Experiments in 3D with ground truth generated by a stereo vision system have been done and yielded promising results. Compared to the state-of-the-art methods, the presented framework uses only half of the required EMT sensors per instrument resulting in significant spatial conservation while improving the catheter shape tracking accuracy by 57%.**

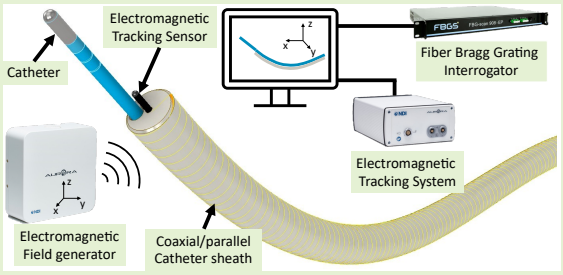

***Index Terms*— Steerable Catheters/Needles, Sensor Fusion, Shape Sensing, Optical Fiber, Electromagnetic Tracking**

I. INTRODUCTION

Modern surgery is increasingly relying on Minimally Invasive Surgery (MIS) [1]. These procedures are beneficial for the patient (faster recovery, shorter hospital stay, and cosmetic aspects) but they are much more challenging to perform for the physicians. In minimally invasive catheter-based interventions, long and slender instruments are inserted through a small incision and are navigated through vessels to reach the operational site. Interventions normally make use of a guidance sheath and a catheter that is coaxial with the sheath. The purpose of the guidance sheath is to offer a stable access route for the catheter toward the anatomical site of interest. At the same time, the sheath shields the fragile anatomy from excessive catheter motion. The latter can move back and forward without needing to worry that fragile regions such as aneurysms undergo excessive stresses, plaque, or calcification get dislodged. Overall, positioning these sheaths or navigating the catheter is hard since there is limited information on the shape and the location of the devices. Current navigation tasks rely heavily on fluoroscopic imaging. Fluoroscopy provides real-time visualization of the instruments but it only offers 2-dimensional (2D) information. Moreover, radiation from fluoroscopic systems is harmful to both patients and clinicians. Due to these reasons, researchers are looking for alternatives [2].

Several sensor modalities have been proposed to be integrated into the catheter to track its shape. Electromagnetic tracking (EMT) sensors are widely studied thanks to their small size and no line-of-sight needed. However, EMT-based catheter tracking methods [3]–[6] require quite a few sensors to reach sufficient tracking accuracy. Consequently, the catheter becomes more complex and fragile. Furthermore, the sensitivity to the presence of ferromagnetic materials affects the tracking accuracy of EMT approaches. A fusion approach that combines each EMT-based estimated shape with fluoroscopic imaging is proposed by Tran *et al.* [7]. This approach,

This work has received funding from the European Union's Horizon 2020 research and innovation programme under grant agreement No. 101017140, the ARTERY project. This work was also supported by CURE a KU Leuven internal project (3E210658).

Xuan Thao Ha is with the Department of Mechanical Engineering, KU Leuven, 3000 Leuven, Belgium, and also with The BioRobotics Institute, Scuola Superiore Sant-Anna, 56025 Pontedera, Italy (e-mail: xuanthao.ha@kuleuven.be).

Di Wu and Fabian Trauzettel are with the Department of Mechanical Engineering, KU Leuven, 3000 Leuven, Belgium, and also with the Faculty of 3mE, TU Delft, 2628 CD Delft, The Netherlands (e-mail: di.wu@kuleuven.be; F.Trauzettel@tudelft.nl).

Mouloud Ourak and Emmanuel Vander Poorten are with the Department of Mechanical Engineering, KU Leuven, 3000 Leuven, Belgium (e-mail: mouloud.ourak@kuleuven.be; Emmanuel.VanderPoorten@kuleuven.be).

Gianni Borghesan is with the Department of Mechanical Engineering, KU Leuven, 3000 Leuven, Belgium, and also with Flanders Make, 3920 Lommel, Belgium (e-mail: gianni.borghesan@kuleuven.be).

Arianna Menciassi is with The BioRobotics Institute, Scuola Superiore Sant–Anna, 56025 Pontedera, Italy (e-mail: arianna.menciassi@santanna.pisa.it).

however, still has the problem of harmful radiation. Another approach fuses EMT-based shape estimation with mechanic catheter model [8]. This approach has a generalization issue since extra effort is required to model each flexible device.

Fiber optical-based shape sensing methods are becoming popular lately [9]–[12]. Thanks to their small size, lightweight, high flexibility, and safety (*i.e.* being free from the risk of electrocution), multi-core Fiber Bragg Grating (FBG) fibers are appealing to be integrated into flexible devices for shape sensing. Multi-core FBG fiber-based shape sensing integrates the curvatures measured at discrete points along the fiber length to reconstruct the 3D shape of the catheter. A major problem in FBG-based shape sensing is that they are not able to discriminate strain caused by twisting from strain caused by bending. The twist is regarded as one of the most significant difficulties in achieving accurate shape reconstruction since even small amounts of twist have a significant influence on the overall shape accuracy. Twisted multi-core fibers have been proposed in the literature [13], [14] to solve this problem. By using a twisted multi-core fiber, it is possible to measure bend-induced strain and twist-induced strain simultaneously. However, the high cost of twisted multi-core fiber prevents it from being widely used in practice. Furthermore, as far as the authors are aware, superior performance has not yet been demonstrated. Another disadvantage of the FBG-based shape sensing method is that it only offers the 3D shape in a local coordinate frame that is fixed with one of the gratings. To track the 3D reconstructed shape in a global coordinate frame, EMT sensors have been proposed to be integrated into the catheter together with a multi-core FBG fiber [15], [16]. Our previous work [17] has shown that the integration of extra EMT sensors does not only help localize the reconstructed shape in a fixed coordinate frame but also improves the shape sensing accuracy. These works attach at least two EMT sensors to each multi-core FBG fiber to allow robust tracking of the shape. However, due to space limitations, it is advisable to minimize the number of sensors. Also if multiple tools are to be tracked such as in systems like MitraClip (Abbott, USA) or multi-arm robot system [18], foreseeing multiple EMT sensors per shape makes them overly complex, costly, and error-prone. Methods that limit the need for a plurality of EMT sensors *e.g.* by distributing the sensors across the plurality of bodies could be highly advantageous in this context.

This work proposes a new method to track the shapes of a plurality of flexible instruments that are arranged in a coaxial/parallel manner in a global coordinate frame (EMT coordinate frame). So far as the authors are aware, this is the first work that tracks and fuses multiple instrument shapes by distributing a minimal amount of sensors across the plurality of coaxial instruments. Each flexible instrument is equipped with a multi-core FBG fiber and a 5 degree-of-freedom (DOF) EMT sensor at the tip. The multi-core FBG fiber can be placed in the center or in an off-centered position. The proposed method is demonstrated on a system including a 3D-printed flexible guidance sheath specifically designed to accommodate a catheter in an off-centered channel and a commercial ablation catheter. For the sake of simplicity, the term ”coaxial catheter” is consistently employed throughout the text. The method can be easily adapted to other systems where multiple flexible instruments are organized in a parallel fashion (as depicted in Fig. 1). Thus, the plurality of instruments does not need to be strictly coaxial, but could potentially also work for other fixed relations e.g. where one or more shapes are wound in a helicoidal fashion. In catheter systems used in minimally invasive interventions, miniaturization of the devices is expected, and it has also been efficiently actualized across a diverse range of devices. As a consequence, the space between the inner diameter of the guidance sheath and the outer diameter of the catheter is selected such that the inner catheter can slide back and forth inside the guidance catheter with minimal play. In such typical situation, the shapes of both bodies are constrained to remain substantially coaxial to each other. This means that at overlapping sections, the shape of the catheter and the guidance sheath are substantially identical. In this work, this property is utilized to colocate the multiple sensed shapes in the same coordinate frame but also to improve the FBG-based shape sensing accuracy. The fusion of the shapes is also shown to be advantageous to compensate for twist-induced disturbances. Dynamic 3D experiments with ground truth generated by a stereo vision system were done to verify the performance of the proposed coaxial catheter localization and fusion framework.

The rest of the paper is organized as follows: Section II details the newly proposed coaxial catheter localization method and the fusion framework. The validation experiments are described in Section III. Finally, Section IV concludes the work and sketches some future directions.

II. Methods

In the proposed method, the shape of each flexible instrument is estimated by a multi-core FBG fiber. FBG-based shape sensing method relies on discrete curvature measurements made along the length of a fiber. These curvatures are obtained by employing an interrogator that measures the change in the reflected wavelength of each grating. Traditional FBG-based shape sensing methods subsequently integrate the measured curvatures to reconstruct the 3D shape of the fiber. The proposed coaxial catheter localization method starts with reconstructing the shape of the guidance sheath as well as the shape of the catheter in their local coordinate frames $\{sh\}$ and $\{ca\}$, respectively. Such traditional FBG-based shape sensing method is briefly described in Section II-A. After that, the information provided by the EMT sensors attached at the tip of the guidance sheath and the catheter is incorporated to localize the two reconstructed shapes in the global EMT coordinate frame. The coaxial localization method is detailed in Section II-B. The new approach to fuse the shapes computed from the individual fibers while taking into account the pose information offered by the two EMT sensors is explained in Section II-C. The notations used in this paper are summarized in Table I.

A. Traditional FBG-based Shape Sensing Method

The conventional FBG-based shape sensing method relies on strain measured by gratings distributed along the length of

TABLE I
TABLE OF NOTATIONS

λ_B	Current Bragg wavelength
λ_{B_0}	Bragg wavelength measured in the unstrained state
$\Delta\lambda$	Wavelength shift
ΔT	Change of the environment temperature
ϵ	Mechanical strain applied on the FBG
S_ϵ	Strain sensitivity coefficient
S_T	Temperature sensitivity coefficient
ϵ_{Bend_i}	Bend-induced strain applied on the surrounding cores
κ	Curvature
θ_b	Angle of the bending plane
θ_i	Angle of the i^{th} surrounding cores corresponding to the x-axis of the fiber
r	Distance between the surrounding core and the central core
$\mathbf{i}, \mathbf{j}$	Unit vectors along the x- and y-axes of the fiber cross-section, respectively
s	Arc length variable
$\mathbf{t}$	Tangent vector
$\mathbf{n}$	Normal vector
$\mathbf{b}$	Binormal vector
$\mathbf{x}(s)$	3D Position of a point at arc length s along the reconstructed fiber shape
$\mathbf{T}(s)$	Pose of a point at arc length s along the center line of the reconstructed shape
L_{sh}, L_{ca}	Fiber sensitivity lengths of the guidance sheath and the catheter, respectively
s_i, s_j	Arc length variables of the guidance sheath and the catheter, respectively
$\{sh\}$	Sheath's base frame
$\{ca\}$	Catheter's base frame
$\{ch\}$	Off-centered channel of the sheath's base frame
$\{em\}$	Fixed EMT global coordinate frame
θ_f	Angle between the x-axis of the fiber in the central channel and the center of the off-centered channel
d_f	Distance between the off-centered channel and the center line of the sheath
$g(.)$	Function that maps the curvature of the guidance sheath's center line κ_{sh} to the off-centered channel's center line κ_{ch}
$\mathbf{I}_{3\times3}$	Identity matrix
$s_{i_{EMT}}, s_{j_{EMT}}$	Correspondence arc length of the EMT sensor attached to the guidance sheath and the catheter, respectively
${}^{em}\mathbf{p}_{ca}, {}^{em}\mathbf{p}_{sh}$	Position vectors of EMT sensors attached to the catheter and guidance sheath expressed in $\{em\}$, respectively
${}^{em}\mathbf{t}_{ca}, {}^{em}\mathbf{t}_{sh}$	Tangent vectors of EMT sensors attached to the catheter and guidance sheath expressed in $\{em\}$, respectively
${}^2_1\mathbf{T}$	Transformation matrix from coordinate frame $\{1\}$ to $\{2\}$
$s_{i_{st}}, s_{i_{en}}$	Starting and ending arc length of the overlap section of the sheath, respectively
$s_{j_{st}}, s_{j_{en}}$	Starting and ending arc length of the overlap section of the catheter, respectively
α	Angle between ${}^{sh}n_{ca}(1)$ and ${}^{sh}n_{ch}(s_{i_{st}})$
$\mathbf{b}(t)$	Bezier curve
t	Arc length variable of the Bezier curve where $t \in [0; 1]$
n	Degree of the Bezier curve
$\mathbf{p}_{c_i}$	Control points of the Bezier curve
E_{length}	The difference between the length of the estimated Bezier curve and the arc length between the two EMT sensors
E_κ	The difference between the curvature of the estimated Bezier curve and the curvature measured by the FBG sensors
γ, β	Scaling factors that regulate the relative weight of E_{length} and E_κ, respectively
$\mathbf{x}_{re}(t)$	The shape of the remaining section estimated by the EMT and FBG approach proposed in [17]

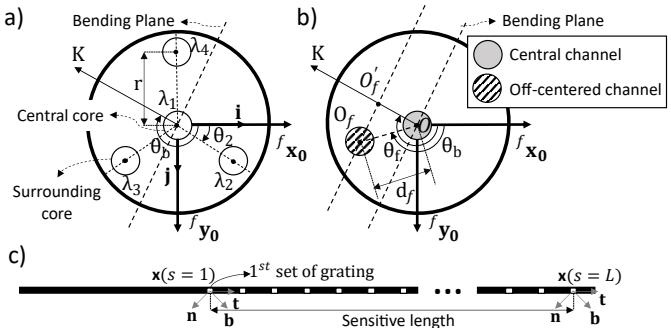

Fig. 1. Cross section view of the multi-core FBG fiber and the guidance sheath can be seen in (a) and (b), respectively. The distance between the central and the surrounding core is defined as $\boldsymbol{r}$. The angle of the bending plane and the angle of the $\mathbf{2^{nd}}$ core with respect to the x-axis are denoted as $\boldsymbol{\theta_b}$ and $\boldsymbol{\theta_2}$, respectively. The distance between the center of the guidance sheath and the off-centered channel central axis is denoted as $\boldsymbol{d_f}$. The angle between the x-axis of the fiber in the central channel and the center of the off-centered channel $\boldsymbol{O_f}$ is $\boldsymbol{\theta_f}$. The fiber sensitive length shown in (c) starts at the first set of grating and ends at the last set of grating.

each optical fiber. Each grating is a Bragg reflector that reflects a particular wavelength of incoming light while transmitting the other wavelengths. The central wavelength of the reflected light of each grating is named the Bragg wavelength λ_B. The Bragg wavelength can be measured by an interrogator connected to the proximal end of the optical fiber. The reflected wavelength of each grating is affected by temperature ΔT and mechanical strain ϵ applied on the fiber. The relation between the wavelength shift $\Delta\lambda$, the change in surrounding temperature ΔT and the applied mechanical strain ϵ is given by:

$$\frac{\lambda_B - \lambda_{B_0}}{\lambda_{B_0}} = \frac{\Delta\lambda}{\lambda_{B_0}} = S_\epsilon\epsilon + S_T\Delta T, \tag{1}$$

where λ_{B_0} is the Bragg wavelength of the grating while it is in the unstrained state. The strain and temperature sensitivity coefficients are denoted as S_ϵ and S_T, respectively. A multi-core FBG fiber used for 3D shape sensing normally features four cores which consists of three surrounding cores and one central core as can be seen in Fig. 1(a). The central core coincides with the neutral axis of the fiber. This core is used to compensate for the axial strain and temperature variations since the wavelength shift of the central core is only sensitive to these two factors. When the axial strain is negligible, as is often the case with catheters, the wavelength shifts caused by temperature changes can be calculated using this central core. The bending strain applied on the surrounding cores $\epsilon_{Bend_{i\in\{2,3,4\}}}$ can then be computed as:

$$\epsilon_{Bend_{i\in\{2,3,4\}}} = \frac{\Delta\lambda_i}{\lambda_{B_{0_i}} S_\epsilon} - \frac{\Delta\lambda_1}{\lambda_{B_{0_1}} S_\epsilon}. \tag{2}$$

At each cross section, where a set of gratings is present, three bend-induced strains in different directions can be calculated. The relations between the curvature κ, the angle of bending plane θ_b, and the three calculated bend-induced strains at a given point are defined as follows:

$$\epsilon_{Bend_{i\in\{2,3,4\}}} = -\kappa r \sin\left(\theta_b - \frac{3\pi}{2} - \theta_i\right), \tag{3}$$

where θ_i is the angle of the i^{th} core corresponding to the x-axis of the fiber; r is the distance from the surrounding core to the central core as depicted in Fig. 1(a). A closed-form solution proposed by Moore and Rogge [11] can be used to solve for the curvature κ and the angle of the bending plane θ_b as below:

$$\begin{aligned} \kappa_{app} &= \sum_{i=2}^{4} \frac{\epsilon_{Bend_i}}{r} \cos\theta_i \mathbf{i} - \sum_{i=2}^{4} \frac{\epsilon_{Bend_i}}{r} \sin\theta_i \mathbf{j}, \\ \kappa_{FBG} &= \frac{2|\kappa_{app}|}{3}, \\ \theta_{b_{FBG}} &= \angle\kappa_{app}, \end{aligned} \tag{4}$$

where $\mathbf{i}$ and $\mathbf{j}$ are the unit vectors along the x- and y-axes of the fiber's cross section (as shown in Fig. 1(a)), respectively.

In the traditional FBG-based shape sensing method, the 3D shape of the fiber is represented by a continuous and differentiable space curve. A space curve is described by curvature $\kappa(s)$ and torsion $\tau(s)$ profiles, where s is the variable arc length. Assuming that the sensitive length of the fiber is discretized into L points, s varies from 1 to L. The fiber sensitive length L starts at the first set of grating and ends at the last set of grating as shown in Fig. 1(c). Torsion $\tau(s)$ is the rate of change of the angle of the bending plane θ_b along the fiber length s. To enhance the approximated form, the set of discrete curvatures and the angles of the bending plane are first interpolated. For each length s, a local coordinate frame with axis TNB is attached rigidly to the fiber. The evolution of the tangent $\mathbf{t}$, normal $\mathbf{n}$, and binormal $\mathbf{b}$ unit vectors (TNB frame) along the fiber arc length is determined by the estimated curvature and torsion profiles. In this work, the differential Frenet - Serret formula [19] is used to solve for the evolution of the TNB frame. Finally, the position vector $\mathbf{x}(s)$ of each point along the fiber shape in the fiber's base frame fixed to the most proximal grating can be calculated by integrating the tangent unit vectors as follows:

$$\mathbf{x}(s) = \mathbf{x}(1) + \int_1^s \mathbf{t}(z)dz, \tag{5}$$

where $\mathbf{x}(1)$ is the position of the fiber's base.

B. Coaxial Catheter Localization Method

The guidance sheath is sensorized by inserting a multi-core FBG fiber into its central channel. To further localize the 3D sheath shape in the EMT coordinate frame, an EMT sensor is attached to the tip of the guidance sheath. Similarly, the catheter is equipped with a multi-core fiber in the central channel and an EMT sensor at the tip. The two EMT sensors are positioned along the center line of the guidance sheath and the catheter.

In an arbitrary situation, the guidance sheath may take on an arbitrary 3D shape, *e.g.* conforming to the shape of a surrounding vessel. The said shape is typically expressed by formulating the geometric shape of the center line ${}^{sh}\mathbf{x}_{sh}(s_i)$ and the set of tangent ${}^{sh}\mathbf{t}_{sh}(s_i)$, normal ${}^{sh}\mathbf{n}_{sh}(s_i)$ and binormal ${}^{sh}\mathbf{b}_{sh}(s_i)$ unit vectors with respect to the sheath's base frame $\{sh\}$. For a guidance sheath that has a sensing length of L_{sh}, s_i varies from 1, at the proximal end of the sheath, to L_{sh}, at the distal end of the sheath. The pose of each point along the center line of the guidance sheath is denoted as ${}^{sh}\mathbf{T}_{sh}(s_i)$, where $\mathbf{T}(s) = \begin{bmatrix} \mathbf{t}(s) & \mathbf{n}(s) & \mathbf{b}(s) & \mathbf{x}(s) \\ 0 & 0 & 0 & 1 \end{bmatrix}$.

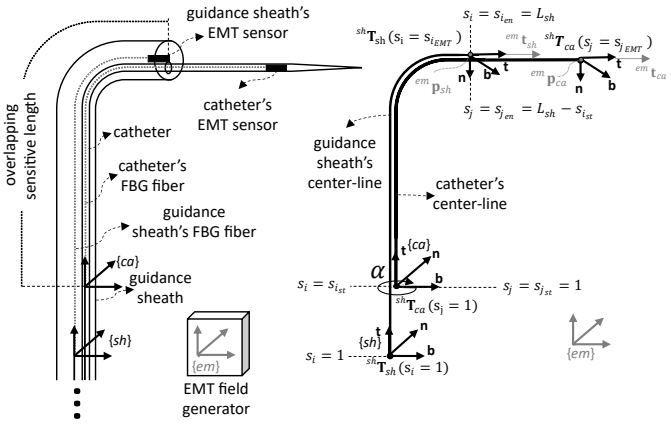

Fig. 2. The reconstructed shape of the catheter is localized in the sheath base frame{sh}. The overlapping length of the guidance sheath starts at $s_i = s_{i_{st}}$ and ends at $s_i = s_{i_{en}}$ while that of the catheter starts at $s_j = s_{j_{st}}$ and ends at $s_j = s_{j_{en}}$. The sensitive length of the two fibers is shown in the dashed gray lines.

Along similar lines, the 3D shape of the catheter can be expressed in its local reconstructed frame with respect to the base frame $\{ca\}$. The pose of each point along the center line of the catheter is denoted as ${}^{ca}\mathbf{T}_{ca}(s_j)$. The arc length s_j of the catheter varies from 1, at the proximal end to L_{ca}, at the distal end of the sensing length of the catheter.

It is worth mentioning that in practice, the working channel of the guidance sheath through which the catheter enters is not necessarily in the center of the guidance sheath. In a more general case, the catheter thus moves in an off-centered channel. In this case, the center line of the off-centered channel of the guidance sheath (expressed in the sheath base frame $\{sh\}$) ${}^{sh}\mathbf{T}_{ch}(s_i)$ should be calculated and used in this catheter localization process. The relation of the guidance sheath center line's curvatures and the off-centered channel center line's curvatures is given by

$$\begin{aligned} \kappa_{ch} = g(\kappa_{sh}) &= \left({\kappa_{sh}}^{-1} - \frac{\overrightarrow{OO_f'} \cdot \overrightarrow{OK}}{||\overrightarrow{OK}||} \right)^{-1}, \\ \theta_{b_{ch}} &= \theta_{b_{sh}}, \end{aligned} \tag{6}$$

where κ_{sh} and $\theta_{b_{sh}}$ are the curvatures and the angles of the bending plane of the center line of the guidance sheath measured by the multi-core FBG fiber, respectively. The curvatures and the angles of the bending plane of the center line of the off-centered channel of the guidance sheath are denoted as κ_{ch} and $\theta_{b_{ch}}$, respectively. The projection of O_f (center of the off-centered channel) on the bending direction vector $\overrightarrow{OK}$ is denoted as O_f'. The relative position of the off-centered channel O_f and the center line of the guidance sheath O is characterized by the distance to the center line d_f and the angle θ_f between $\overrightarrow{OO_f}$ and the x-axis. The relation between these parameters can be seen in the cross sectional view of the guidance sheath shown in Fig. 1(b). A pre-calibration needs to be done in advance to identify the two parameters d_f and

θ_f. This pre-calibration procedure is presented in Section III. The pose of each point along the length of the off-centered channel's center line ${}^{ch}\mathbf{T}_{ch}(s_i)$ with respect to its base frame $\{ch\}$ can be estimated by integrating the calculated κ_{ch} and $\theta_{b_{ch}}$. A transformation matrix ${}^{sh}_{ch}\mathbf{T}$ that transforms the off-centered channel shape in its base frame $\{ch\}$ to the sheath base frame $\{sh\}$ can then be calculated as:

$$ {}^{sh}_{ch}\mathbf{T} = \begin{bmatrix} & \mathbf{I_{3\times 3}} & & -d_f\, cos(\theta_f) \\ & & & -d_f\, sin(\theta_f) \\ & & & 0 \\ 0 & 0 & 0 & 1 \end{bmatrix}. \tag{7} $$

To localize the reconstructed 3D shape of the catheter in the $\{sh\}$ frame, a transformation matrix ${}^{sh}_{ca}\mathbf{T}$ needs to be determined. Since the catheter can move backward and forward inside the off-centered tubular structure of the sheath, the origin of the catheter's base frame moves along the off-centered channel's shape in $\{sh\}$. The origin of the catheter's base frame is always aligned with a point at arc length $s_{i_{st}}$. The arc length $s_{i_{st}}$ varies over time during insertion and retraction. This means that ${}^{sh}\mathbf{x}_{ca}(1) = {}^{sh}\mathbf{x}_{ch}(s_{i_{st}})$ and ${}^{sh}\mathbf{t}_{ca}(1) = {}^{sh}\,\mathbf{t}_{ch}(s_{i_{st}})$. The normal vector ${}^{sh}\mathbf{n}_{ca}(1)$ and binormal vector ${}^{sh}\mathbf{b}_{ca}(1)$ can be obtained by rotating ${}^{sh}\mathbf{n}_{ch}(s_{i_{st}})$ and ${}^{sh}\mathbf{b}_{ch}(s_{i_{st}})$ around ${}^{sh}\mathbf{t}_{ch}(s_{i_{st}})$ by an angle α, respectively. Given the pose of the origin of the catheter's base expressed in its base frame ${}^{ca}\mathbf{T}_{ca}(1)$ and in the sheath frame ${}^{sh}\mathbf{T}_{ca}(1)$, a transformation matrix ${}^{sh}_{ca}\mathbf{T}$ that transforms the catheter shape from its base frame $\{ca\}$ to the sheath frame $\{sh\}$ can be calculated by using a point-to-point registration method [20].

By knowing ${}^{sh}_{ca}\mathbf{T}$, both the catheter and the guidance sheath shape can be further localized in the EMT coordinate frame $\{em\}$. Since the EMT manufacturer normally does not provide the actual location of the EMT sensor body that is being measured, a spatial calibration step is required to determine the correspondence of the measurement point of the EMT sensors and the FBG-based 3D reconstructed shape. The spatial calibration can be conducted by fixing the catheter on a planar plane and subsequently bending the catheter into two symmetric configurations. The travel distance of the EMT sensor and the travel distance of each point along the length of the two reconstructed shapes is then compared to find the measurement point of the EMT sensor. By this spatial calibration step, the correspondence arc lengths of the EMT sensors attached to the guidance sheath ($s_{i_{EMT}}$) and to the catheter ($s_{j_{EMT}}$) can be obtained. Details on this spatial calibration process can be found in [16]. By knowing $s_{i_{EMT}}$ and $s_{j_{EMT}}$, four points in the sheath base frame $\{sh\}$

$$ \begin{aligned} \mathbf{a} = [& {}^{sh}\mathbf{x}_{ca}(s_{j_{EMT}}) \quad {}^{sh}\mathbf{x}_{ca}(s_{j_{EMT}}) + {}^{sh}\,\mathbf{t}_{ca}(s_{j_{EMT}}) \\ & {}^{sh}\mathbf{x}_{sh}(s_{i_{EMT}}) \quad {}^{sh}\mathbf{x}_{sh}(s_{i_{EMT}}) + {}^{sh}\,\mathbf{t}_{sh}(s_{i_{EMT}})] \end{aligned} \tag{8} $$

together with their corresponding points in the EMT coordinate frame $\{em\}$

$$ \mathbf{b} = \begin{bmatrix} {}^{em}\mathbf{p}_{ca} & {}^{em}\mathbf{p}_{ca} + {}^{em}\,\mathbf{t}_{ca} & {}^{em}\mathbf{p}_{sh} & {}^{em}\mathbf{p}_{sh} + {}^{em}\,\mathbf{t}_{sh} \end{bmatrix} \tag{9} $$

can be used to perform a point-to-point registration [20] and to calculate the transformation matrix ${}^{em}_{sh}\mathbf{T}$ that transforms the shapes reconstructed in $\{sh\}$ to $\{em\}$. The vectors ${}^{em}\mathbf{p}_{ca}$ and ${}^{em}\mathbf{t}_{ca}$ are the position and the unit tangent vector measured by the EMT sensor attached to the tip of the catheter, respectively. Similarly, the position and tangent vector of the EMT sensor attached to the tip of the sheath are defined as ${}^{em}\mathbf{p}_{sh}$ and ${}^{em}\mathbf{t}_{sh}$, respectively.

The relation between the poses of the shape at the level (arc length $s_{i_{EMT}}$ and $s_{j_{EMT}}$) of the EMT sensors should in principle be identical to the relation between the poses of the EMT sensors themselves. Thus, an optimization problem can be formulated to find the two unknowns $s_{i_{st}}$ and α to derive ${}^{sh}\mathbf{T}_{ca}(1)$ by minimizing the following cost function

$$ \underset{s_{i_{st}},\alpha}{\arg\min} \, ||{}^{em}_{sh}\mathbf{T}\ \mathbf{a} - \mathbf{b}||. \tag{10} $$

The two parameters $s_{i_{st}}$ and α are varied to find optimal values that minimize the registration error of the two point clouds **a** and **b**. Figure 2 shows the reconstructed shape of the catheter in the guidance sheath base frame $\{sh\}$.

C. Fusion Framework for Coaxial Catheter

One of the disadvantages of a straight multi-core fiber compared to a helical configuration in shape sensing is that it cannot distinguish strain induced by twisting from strain induced by bending. To avoid this ambiguity, catheters are normally made from torsionally stiff elements to prevent torsion. In practice, it is very difficult to design a catheter that protects the fiber completely from torsion. Given that even small amounts of twists have a large impact on the overall shape accuracy, the twist is considered one of the most important challenges to achieving precise shape reconstruction. The second disadvantage of traditional FBG-based shape sensing methods follows from the fact that the 3D shape is reconstructed by integrating the measured curvature along the fiber length. By doing so, the curvature measurement error accumulates along the length, therefore the highest shape sensing error typically appears at the fiber tip which happens to be the most interesting point one wants to know precisely. By using a coaxial catheter system (*i.e.* a guidance sheath and a catheter), it is possible to address these problems. Since the catheter and the sheath are coaxial, the shape of the overlapping section of the catheter and the sheath should be identical. The remaining distal section of the catheter or guidance sheath is constrained by the two EMT sensors depending on the relative position of the catheter with respect to the guidance sheath as can be seen in Fig. 3. In this section, a fusion framework that uses the two aforementioned characteristics to enhance the guiding sheath and catheter's shape sensing accuracy is presented. During the procedure, the catheter moves inside the guidance sheath's channel, the overlapping section can be determined by knowing the length of the two reconstructed shapes and $s_{i_{st}}$. Assuming that the sensed length of the catheter is shorter than that of the guidance sheath ($L_{ca} < L_{sh}$) and $s_{i_{st}} \geq 1$ during the procedure, the relative position of the catheter with respect to the guidance sheath's channel can belong to one of two cases. In the first case, the length of the catheter is entirely covered by the guidance sheath's channel. In other words, the tip of the catheter moves inside the channel of the guidance sheath. In the second case, the tip of the catheter moves out of the guidance sheath. The arc length of the overlapping section

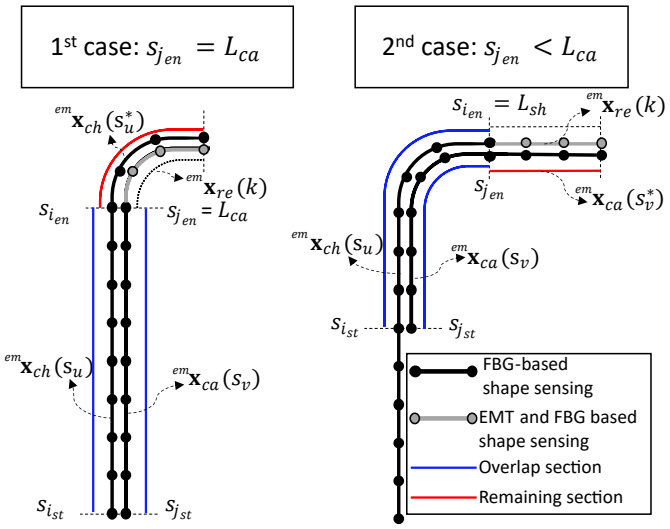

Fig. 3. In the here proposed fusion framework, the catheter shape is approximated by a Bezier curve that matches best with the shapes estimated by the different sensors. The black lines show the shapes estimated by the traditional FBG-based shape sensing method while the gray lines show the shapes estimated by EMT and FBG-based shape sensing method [17].

of the sheath (starts at $s_{i_{st}}$ and ends at $s_{i_{en}}$) and of the catheter (starts at $s_{j_{st}}$ and ends at $s_{j_{en}}$) as shown in Fig. 3 can be found by Algorithm 1.

Algorithm 1 Overlapping section arc length calculation for the guidance sheath and the catheter

if $s_{i_{st}} + L_{ca} \geq L_{sh}$ **then**
  $s_{i_{en}} = L_{sh}$
else
  $s_{i_{en}} = s_{i_{st}} + L_{ca}$
end if
$s_{j_{st}} \leftarrow 1$
if $L_{sh} - s_{i_{st}} \geq L_{ca}$ **then**
  $s_{j_{en}} = L_{ca}$
else
  $s_{j_{en}} = L_{sh} - s_{i_{st}}$
end if

In theory, the shape of the overlapping section in the EMT coordinate frame should be identical $^{em}\mathbf{x}_{ch}(s_u) = {}^{em}\mathbf{x}_{ca}(s_v)$ where $s_u = \{s_{i_{st}}, ..., s_{i_{en}}\}$ and $s_v = \{s_{j_{st}}, ..., s_{j_{en}}\}$. However, this is not true in practice due to the problem of curvature measurement error accumulation and dynamic twist that is applied to the fiber. A fusion framework is proposed to overcome this issue. In the here proposed fusion framework, the shape of the guidance sheath's channel and the catheter are approximated by two Bezier curves. A Bezier curve of degree n in the $\{em\}$ frame can be specified by $n+1$ control points and is defined as

$$^{em}\mathbf{b}(t) = \sum_{i=0}^{n} \binom{n}{i} (1-t)^{n-i} t^i \, {}^{em}\mathbf{p}_{c_i} \tag{11}$$

where $\binom{n}{i}$ are the binomial coefficients and $t \in [0;1]$. Vectors $^{em}\mathbf{p}_{c_i}$ are the control points.

The general idea is to find a Bezier curve that matches best with the shapes estimated by the different sensors. The shape of the overlapping section - this refers to the common section where its shape can be measured by both fibers - will be fused by the two shapes $^{em}\mathbf{x}_{ch}(s_u)$ and $^{em}\mathbf{x}_{ca}(s_v)$. The remaining section will be fused between the shape estimated by the traditional approach and our novel EMT and FBG-based shape sensing approach presented in [17]. The remaining section in the first case is the shape of the sheath $^{em}\mathbf{x}_{ch}(s_u^*)$ starting from arc length $s_i = s_{i_{en}}+1$ up to arc length $s_i = L_{sh}$ ($s_u^* = \{s_{i_{en}+1}, ..., L_{sh}\}$). In the second case, the remaining section is the part of the catheter that extends beyond the sheath $^{em}\mathbf{x}_{ca}(s_v^*)$ starting from arc length $s_j = s_{j_{en}}+1$ up to $s_j = L_{ca}$ ($s_v^* = \{s_{j_{en}+1}, ..., L_{ca}\}$). The overlap section and the remaining section of the first and the second are denoted by the blue and red lines in Fig. 3, respectively.

Note that the shape of the remaining section can be estimated using the method proposed in [17] since it has the two EMT sensors constraining the two ends and the discrete curvatures along the length obtained from the FBG sensors. In the EMT and FBG-based shape sensing method [17], the shape of the catheter segment between the two EMT sensors is represented by a Bezier curve. The first and the last control points of the Bezier curve are defined by the positions of the two EMT sensors. An optimization problem is formulated to find the remaining control points by minimizing the cost function

$$\underset{\mathbf{p}_{c_1},...,\mathbf{p}_{c_{n-1}}}{\arg\min} \quad \gamma E_{length} + \beta E_{\kappa} \tag{12}$$

where γ and β are the two scaling factors that regulate the relative weight of E_{length} and E_{κ}, respectively. The error E_{length} is the difference between the length of the estimated Bezier curve and the arc length between the two EMT sensors. The error in curvature E_{κ} is the difference between the curvature along the length of the estimated Bezier curve and the curvatures obtained from the FBG sensors over the corresponding section. Detailed calculations of these two error terms can be found in [17]. The objective of the optimization problem represented by equation (12) is to ascertain the control points of a Bezier curve that exhibit curvatures consistent with the measurements acquired from FBG sensors, while simultaneously maintaining a length equivalent to the arc distance between the two EMT sensors. The shape of the remaining section in the EMT coordinate frame estimated by the fusion EMT and FBG-based shape sensing method is denoted as $^{em}\mathbf{x}_{re}(t)$ where $t \in [0;1]$.

The overall fused shape in the EMT coordinate frame (including the overlapping section and the remaining section) can now be estimated by approximating the set of points $\mathbf{c}$ by a Bezier curve $\mathbf{b}(t)$. The set of points $\mathbf{c}$ is defined as

$$\mathbf{c} = [{}^{em}\mathbf{x}_{ch}(s_u) \; {}^{em}\mathbf{x}_{ch}(s_u^*) \; {}^{em}\mathbf{x}_{ca}(s_v) \; {}^{em}\mathbf{x}_{re}(k)]^T \tag{13}$$

in the 1^{st} case and

$$\mathbf{c} = [{}^{em}\mathbf{x}_{ca}(s_v) \; {}^{em}\mathbf{x}_{ca}(s_v^*) \; {}^{em}\mathbf{x}_{sh}(s_u) \; {}^{em}\mathbf{x}_{re}(k)]^T \tag{14}$$

in the 2^{nd} case where

$$k = \begin{cases} \frac{s_u^* - s_{i_{en}+1}}{L_{sh} - s_{i_{en}+1}} & \text{in the } 1^{st} \text{ case} \\ \frac{s_v^* - s_{j_{en}+1}}{L_{ca} - s_{j_{en}+1}} & \text{in the } 2^{nd} \text{ case} \end{cases} \tag{15}$$

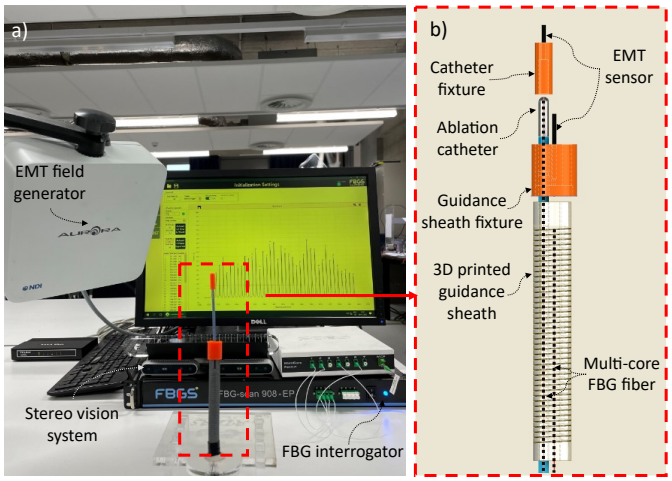

Fig. 4. The experiment setup is shown in (a) including the built catheter system, EMT tracking system, and FBG interrogator. The 3D design of the parallel catheter system is described in (b). The two EMT sensors are attached to the catheter and the guidance sheath by two 3D-printed fixtures. The multi-core fibers are inserted into the central channel of the catheter and the guidance sheath.

The order of the approximated Bezier curve ${}^{em}\mathbf{b}(t)$ is defined depending on the complexity of the estimated shape given that an n^{th} order Bezier curve can only change direction along an axis at most $n-1$ times. To approximate the set of m points $\mathbf{c}$ by a Bezier curve, the matrix form of the Bezier curve, based on the control points, can be used. The control points of 3^{rd} and 4^{th} order Bezier curve that best fit the set of points $\mathbf{c}$ can be calculated by equation (16) and (17), respectively.

$$\begin{bmatrix}\mathbf{p}_{c_0}\\ \mathbf{p}_{c_1}\\ \mathbf{p}_{c_2}\\ \mathbf{p}_{c_3}\end{bmatrix} = \left(\begin{bmatrix}\mathbf{t}^3 & \mathbf{t}^2 & \mathbf{t} & \mathbf{1}\end{bmatrix}\begin{bmatrix}-1 & 3 & -3 & 1\\ 3 & -6 & 3 & 0\\ -3 & 3 & 0 & 0\\ 1 & 0 & 0 & 0\end{bmatrix}\right)^{+}\mathbf{c}_{m\times 3} \tag{16}$$

$$\begin{bmatrix}\mathbf{p}_{c_0}\\ \mathbf{p}_{c_1}\\ \mathbf{p}_{c_2}\\ \mathbf{p}_{c_3}\\ \mathbf{p}_{c_4}\end{bmatrix} = \left(\begin{bmatrix}\mathbf{t}^4 & \mathbf{t}^3 & \mathbf{t}^2 & \mathbf{t} & \mathbf{1}\end{bmatrix}\begin{bmatrix}1 & -4 & 6 & -4 & 1\\ -4 & 12 & -12 & 4 & 0\\ 6 & -12 & 6 & 0 & 0\\ -4 & 4 & 0 & 0 & 0\\ 1 & 0 & 0 & 0 & 0\end{bmatrix}\right)^{+}\mathbf{c}_{m\times 3} \tag{17}$$

where $\mathbf{p}_{c_{i=\{0,\dots,n\}}}$ are the control points of the Bezier curve that approximates the fused shape in the $\{em\}$ frame and the $(.)^{+}$ sign denotes the moore-penrose inverse. The matrix $\mathbf{t}$ is a $m \times 1$ matrix that contains the arc length of each point in $\mathbf{c}$ normalized to the range $[0; 1]$. It is worth noting that while the matrix forms of 3^{rd} order and 4^{th} order Bezier curves are given here as examples, higher order Bezier curves can still be used to approximate more complex shapes depending on applications.

III. EXPERIMENTAL VALIDATION

A. Experimental setup

To validate our proposed coaxial catheter localization method and the fusion framework, 3D experiments are performed. A 3D-printed steerable catheter with an outer diameter of 11 mm and a length of 75 mm (called 3Flex [22]) is employed. The 3D-printed catheter mimics a guidance sheath. It has a central channel that can accommodate a multi-core FBG fiber and an off-centered channel that allows a smaller catheter to be slid through. A multi-core FBG fiber with an outer diameter of 0.38 mm from FBGS (Geel, Belgium) is integrated into the central channel of the 3D-printed guidance sheath. The fiber features four cores with eight gratings distributed along the sensitive length and present at the same arc length for each core (leading to a total of 32 gratings). The spacing between sets of gratings is 14 mm. A 3D-printed fixture is made and is attached to the tip of the guidance sheath to hold the EMT sensor. An 8 Fr ablation catheter from Biosense Webster (Irvine, CA, USA) is guided by the 3Flex. This catheter is inserted into the off-centered channel of the 3D-printed guidance sheath. The ablation catheter fits nicely to the guidance sheath's off-centered channel so that the catheter can simply slide forward and backward. A second 3D-printed fixture is designed to fix an EMT sensor to the tip of the catheter. A multi-core FBG fiber is embedded into the irrigation channel of the ablation catheter. The used multi-core fiber has four cores, each with 22 gratings distributed along it. The distance between two grating sets is 10 mm. In both systems, the FBG fibers are fixed into the respective channels and glued with epoxy glue. The design of the 3D-printed guidance sheath and the proposed method to integrate the fibers and the EMT sensors into the flexible instrument is shown in Fig. 4. In order to mitigate the potential impact of internal bending and twisting that could occur during the insertion of fibers into the instrument channels, as well as the pre-bending of the instrument itself, the calibration procedure for shape sensing, as described in [10], was performed after integration of the fibers.

Two experiments have been carried out in this work. In the first experiment, the catheter was inserted through the off-centered channel of the guidance sheath until the tip of the catheter reached the end point of the guidance sheath. From this point, the catheter was pushed forward and pulled backward manually. The first experiment was designed to validate the proposed coaxial catheter localization method. Thus, there was no bending applied to the catheter during the first experiment. In the second experiment, the catheter was inserted through the guidance sheath's channel until the length of the exited part of the catheter ($L_{ca} - s_{j_{en}}$) was approximately 130 mm. The catheter was then manually bent into different configurations and directions. Since the purpose of this experiment is to show the effectiveness of the proposed fusion framework in improving the shape sensing accuracy, especially in large bending cases, the catheter was bent more than 90 degrees in this experiment. During the experiment, the wavelength shifts of the two multi-core fibers and the poses of the two EMT sensors were recorded to reconstruct the shape of the guidance sheath and the catheter.

B. Off-centered catheter calibration

Since the channel for the catheter is placed off-center, a pre-calibration step is needed to find the two parameters d_f and θ_f. By knowing these two parameters, the curvature along the center line of the off-centered channel can be estimated from the curvature of the fiber in the central channel of the

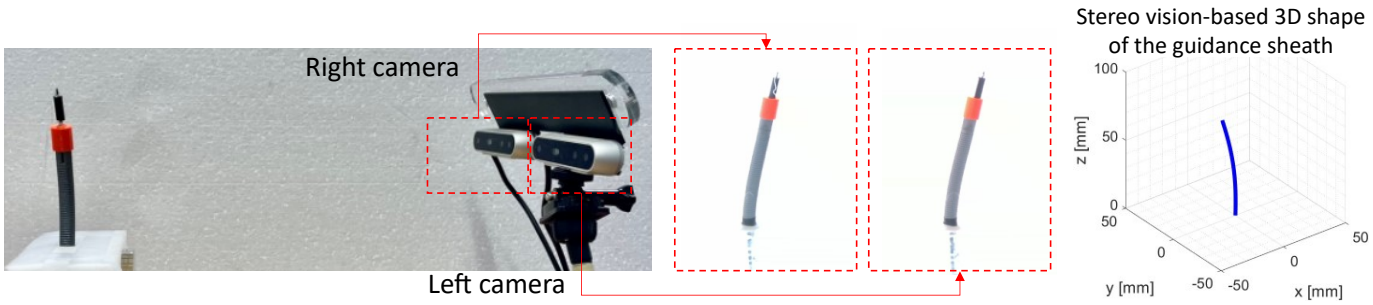

Fig. 5. The 3D shape of the guidance sheath is estimated using the stereo vision system [21]. The EMT and 3D stereo vision coordinate frame are then registered. After that, the estimated shape of the catheter using our proposed method is mapped to the two 2D image frames to calculate the shape estimation error.

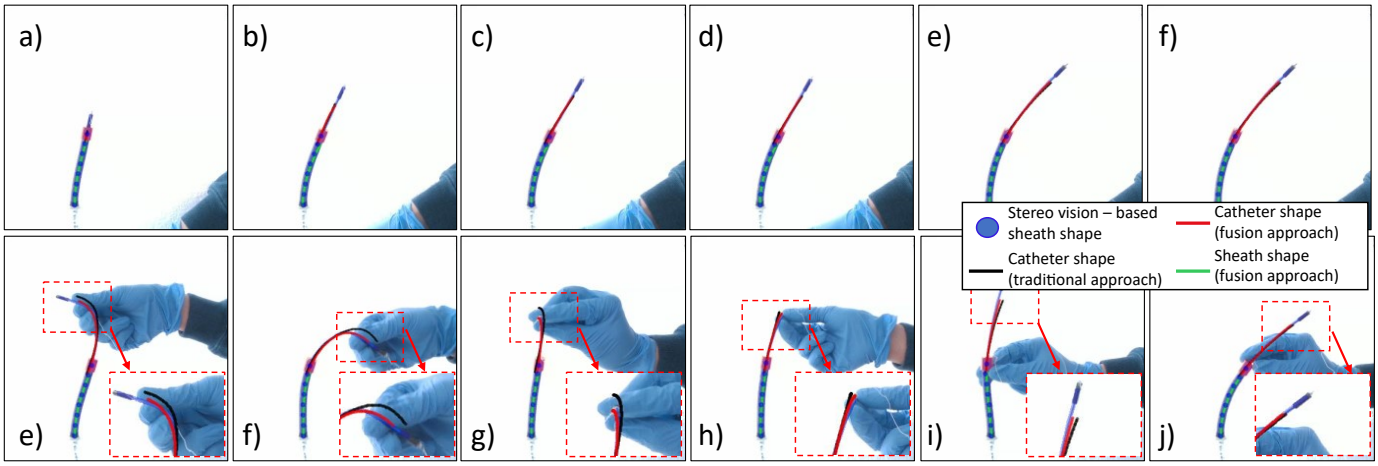

Fig. 6. The 3D estimated shapes of the guidance sheath and the catheter using the proposed fusion approach and the traditional approach in the EMT coordinate frame are projected to the images from the left camera. The ground truth shape of the guidance sheath is shown by the blue circles. The guidance sheath shapes estimated by the proposed fusion approach are plotted in green. The red and black lines show the estimated catheter shape using our proposed fusion approach and the traditional approach, respectively. The experimental results of the first and second experiments can be seen in the images on the first row (a)-(f) and second row (g)-(l), respectively. In the first experiment, the catheter was inserted and retracted without undergoing any bending since this experiment was designed to validate the proposed coaxial catheter localization method. In contrast, the second experiment entailed considerable bending in various directions to show the advantage of the proposed fusion framework.

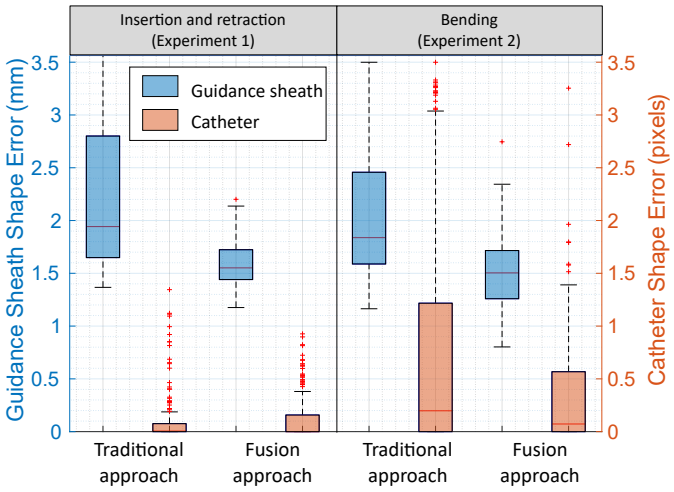

Fig. 7. The quantitative shape tracking results of the two experiments using the traditional approach and our proposed fusion approach. The guidance sheath tracking error (referenced to the left y-axis) is calculated in mm while that of the catheter (referenced to the right y-axis) is calculated in pixels. The scaling relationship between pixels and millimeters depends on the spatial separation between the catheter and the cameras employed. The average conversion factor is determined to be $\mathbf{0.73}$ mm per pixel.

guidance sheath as described in Section II-B. The distance from the center line of the off-centered channel to the center line of the guidance sheath is approximately known by the design. The remaining parameter θ_f is the angle between $\overrightarrow{OO_f}$ and the x-axis of the fiber inserted into the central channel of the guidance sheath. The pre-calibration step starts by first inserting the sensorized catheter into the off-centered channel of the guidance sheath until the tip of the catheter reaches the tip of the guidance sheath. The guidance sheath is then bent in different directions manually. The wavelength shifts of both fibers are recorded during the pre-calibration. By having the catheter in the off-centered channel, the curvatures of the center line of the off-centered channel can be measured. To find the two parameters d_f and θ_f, an optimization problem was formulated by minimizing the following cost function

$$\arg\min_{d_f,\theta_f} \frac{1}{q}\sum_{t=1}^{q} ||g(\kappa_{sh_{calib_t}}) - \kappa_{ca_{calib_t}}||, \qquad (18)$$

where $\kappa_{sh_{calib_t}}$ and $\kappa_{ca_{calib_t}}$ are the set of curvatures measured by the fiber inserted into the sheath and by the fiber inserted into the catheter at time step t^{th}, respectively. The number q is the number of samples recorded during the pre-calibration step (each time step is one sample).

C. Ground truth generation

The ground truth shapes of both the guidance sheath and the catheter were generated using two cameras (Intel RealSense D415) fixed at the same distance from the experimental setup. The experimental setup was placed in front of a white background to enhance the contrast between the catheter shape and the background. The 3D shapes of the guidance sheath were reconstructed using the stereo vision system (shown in Fig. 5) and the epipolar geometry principles as proposed in [21]. The stereo vision system was calibrated using the calibration toolbox from MATLAB (The MathWorks, Inc., Massachusetts, United States). The stereo vision camera calibration process yielded a mean re-projection error of 0.28 pixels. With the method proposed in [21], the 3D shape of the guidance sheath could be recognized in the stereo vision coordinate frame.

At each time step, the 3D guidance sheath shape was estimated by our proposed method and by the stereo vision system. To register the EMT and stereo vision coordinate frames, a point-to-point registration method [20] was used. Once the two coordinate frames are registered, the estimated shape of the catheter using our proposed method can be then mapped to the two 2D image frames. The shape estimation error is calculated by the distance between each point along the mapped catheter shape to the closest point of the catheter's contour in the image frame. The guidance sheath's shape sensing error is calculated by the distance between each point of the estimated shape in the 3D stereo vision coordinate frame to the closest point of the guidance sheath ground truth shape recognized by the stereo vision. The closest points between the two sets of points were found by using the function *dsearchn* [23] provided by MATLAB. Since the catheter shape is compared to its ground truth in the image frame, the unit of the shape sensing error of the catheter is in pixels while that of the guidance sheath is in mm. One may ask about the reason for having different ground truths for the guidance sheath and the catheter shape. During the experiments, the catheter experienced large bending in different directions to show the comprehensiveness of our proposed method. In some bending directions, the full shape of the catheter cannot be captured by the stereo vision system (*e.g.* Fig. 6(i)(j)) which makes it impossible to reconstruct the full 3D catheter ground truth shape. Due to this reason, the estimated catheter shape is projected to the two image frames to calculate the shape tracking error. Unlike the catheter, the full shape of the guidance sheath is always available (since the guidance sheath did not experience large bending during the experiments), allowing for the comparison of the full guidance sheath shape in the 3D stereo vision shape reconstruction coordinate frame. The coaxial catheter localization method without the fusion framework was also implemented to be used as a baseline against which the proposed fusion framework was compared. In these experiments, only the shapes of the guidance sheath were used to register the EMT and the stereo vision shape reconstruction frame instead of using both the sheath shape and the catheter shape. Since the target of these experiments is to track the catheter's shape, this approach helps avoid the problem of actively reducing the error between the estimated catheter shape and its ground truth shape due to the point-to-point registration process.

TABLE II
MEAN ERROR OF THE RECONSTRUCTED SHAPE OF THE GUIDANCE SHEATH (IN MM) AND OF THE CATHETER (IN PIXELS) USING THE TRADITIONAL APPROACH AND THE HERE PROPOSED FUSION APPROACH IN THE EXPERIMENT 2. THE REPORTED SUB-EXPERIMENT 2.1-2.6 CORRESPONDS TO THE BENDING EXPERIMENT IN DIFFERENT DIRECTIONS AS SHOWN IN FIG. 7(E)-(J).

	Guidance Sheath Mean Error (mm)		Catheter Mean Error (pixels)	
	Traditional	Fusion	Traditional	Fusion
Exp 2.1	2.35±0.45	1.80±0.25	2.37±1.68	0.46±0.33
Exp 2.2	1.62±0.24	1.08±0.14	2.27±1.05	0.79±0.37
Exp 2.3	1.68±0.20	1.35±0.22	1.33±1.07	0.72±0.84
Exp 2.4	1.97±0.34	1.53±0.37	1.48±1.42	0.71±1.23
Exp 2.5	2.65±0.61	1.57±0.22	0.94±0.53	0.23±0.31
Exp 2.6	2.11±0.48	1.38±0.23	0.43±0.34	0.15±0.23

D. Results and discussion

Figure 6 shows the 3D estimated catheter shapes using our proposed fusion approach (in red) and the traditional approach (in black) projected in the left camera's images. The ground truth contours of the guidance shape and the catheter are highlighted in blue. The ground truth center lines of the guidance sheath recognized by the stereo vision system are plotted with blue markers. The green lines visualize the shapes of the guidance sheath estimated by the proposed method. The results of both experiments can be found in the attached video. The quantitative shape tracking results of the two experiments are described in Fig. 7. It can be seen that the guidance sheath mean shape sensing accuracy improves by 26% in the catheter insertion experiment (experiment 1). The same trend can be seen in the catheter bending experiment (experiment 2). This shows the potential of the proposed coaxial catheter localization method. The mean catheter shape tracking error of the traditional approach and the fusion approach in the first experiment is similar. Unlike the first experiment, an improvement of 57% can be seen in the second experiment. The catheter shape tracking error of both the traditional approach and fusion approach of the second experiment is larger than that of the first experiment. This discrepancy can be attributed to bending, which may further result in a fiber twist. However, such an issue could potentially be mitigated by the newly proposed method. Detailed results of each sub-experiment in the catheter bending experiment can be found in Table II. The results in this tabular representation indicate that the fusion approach employed in guidance sheath and catheter shape sensing exhibits notably lower mean error and standard deviation values compared to the traditional approach. The problem of having the largest shape sensing error at the catheter tip has been mitigated by our proposed fusion framework by fusing the shape estimated by the traditional approach with the approach proposed in [17]. In the second experiment, the mean of max catheter shape sensing error reduces from 3.9 to 2.5 pixels (approximately 36%). The current proposed framework is implemented on MATLAB and can run at 10 Hz.

It is worth noting that owing to the fact that the catheter and its ground truth shapes were not aligned by using the

Iterative Closest Point (ICP) approach, the reported catheter shape tracking accuracy in our paper might be larger than other works in the art which use ICP [10], [24], [25]. Using ICP is avoided in this work since this registration approach will actively reduce the error between the estimated and its ground truth shapes. The two coordinate frames (EMT frame and 3D stereo vision shape reconstruction frame) were registered using the shape of the guidance sheath only. The error in the shape sensing accuracy of the guidance sheath and the catheter was characterized in different units in this work. Therefore, the accuracy of the catheter and the guidance sheath tracking are not comparable. These experimental results reflect the superiority of the proposed fusion framework compared to the traditional model approach (no fusion) in combination with the coaxial catheter localization method.

IV. CONCLUSIONS

In this paper, a new approach allows tracking the shapes of a plurality of flexible instruments that are arranged in a coaxial manner using a minimal number of sensors. Compared to the traditional approaches [15], [16] in which at least two EMT sensors are required to localize the shape of the catheter in a global coordinate frame (EMT coordinate frame). The approach herein described may co-localize multiple coaxial shapes in the same EMT coordinate frame by exploiting the coaxial property. Thanks to this property, the proposed method only requires one EMT sensor mounted to the tip of each multi-core fiber. This reduces the complexity and the cost of the catheter fabrication process as well as improves the robustness of the catheter tracking system. A fusion approach is also described in this paper to improve catheter shape tracking accuracy. The presented fusion method helps compensate for the twist applied to the fiber during tracking.

Experiments in 3D have been done to verify the two proposed methods with ground truth generated by the stereo vision system. The results show that the proposed coaxial catheter localization method can co-localize the guidance sheath and catheter shapes in the same coordinate frame. The described fusion approach helps improve the catheter shape tracking accuracy by 57% compared to the traditional approach in which only the coaxial catheter localization method is used. In the future, we aim to complement and strengthen our observed findings by conducting animal trials. These trials will be instrumental in assessing the in-vivo performance of our proposed coaxial catheter tracking algorithm, in conjunction with the fusion framework we have presented. In contrast to in-lab experiments, where 3D ground truth shapes can be obtained using a stereo-vision camera, we plan to generate ground truth data using a biplane fluoroscopic system [26]. As in-vivo experiments involve animal subjects and raise ethical considerations, we are planning to collaborate with medical experts and institutions to ensure the execution of rigorous and responsible in-vivo studies.

REFERENCES

[1] G. G. Hamad and M. Curet, "Minimally invasive surgery," *The American Journal of Surgery*, vol. 199, no. 2, pp. 263–265, 2010.

[2] C. Shi, X. Luo, P. Qi, T. Li, S. Song, Z. Najdovski, T. Fukuda, and H. Ren, "Shape sensing techniques for continuum robots in minimally invasive surgery: A survey," *IEEE Transactions on Biomedical Engineering*, vol. 64, no. 8, pp. 1665–1678, 2016.

[3] S. Song, Z. Li, H. Yu, and H. Ren, "Electromagnetic positioning for tip tracking and shape sensing of flexible robots," *IEEE Sensors Journal*, vol. 15, no. 8, pp. 4565–4575, 2015.

[4] S. Song, Z. Li, M. Q.-H. Meng, H. Yu, and H. Ren, "Real-time shape estimation for wire-driven flexible robots with multiple bending sections based on quadratic bézier curves," *IEEE Sensors Journal*, vol. 15, no. 11, pp. 6326–6334, 2015.

[5] X. T. Ha, I. Tamadon, M. Ourak, G. Borghesan, A. Menciassi, and E. Vander Poorten, "Comparative study on electromagnetic tracking and fiber bragg grating-based catheter shape sensing," in *2022 IEEE Sensors*. IEEE, 2022, pp. 1–4.

[6] A. M. Franz, T. Haidegger, W. Birkfellner, K. Cleary, T. M. Peters, and L. Maier-Hein, "Electromagnetic tracking in medicine—a review of technology, validation, and applications," *IEEE transactions on medical imaging*, vol. 33, no. 8, pp. 1702–1725, 2014.

[7] P. T. Tran, P.-L. Chang, H. De Praetere, J. Maes, D. Reynaerts, J. V. Sloten, D. Stoyanov, and E. Vander Poorten, "3d catheter shape reconstruction using electromagnetic and image sensors," *Journal of Medical Robotics Research*, vol. 2, no. 03, p. 1740009, 2017.

[8] A. Dore, G. Smoljkic, E. Vander Poorten, M. Sette, J. Vander Sloten, and G.-Z. Yang, "Catheter navigation based on probabilistic fusion of electromagnetic tracking and physically-based simulation," in *2012 IEEE/RSJ International Conference on Intelligent Robots and Systems*. IEEE, 2012, pp. 3806–3811.

[9] F. Khan, A. Denasi, D. Barrera, J. Madrigal, S. Sales, and S. Misra, "Multi-core optical fibers with bragg gratings as shape sensor for flexible medical instruments," *IEEE sensors journal*, vol. 19, no. 14, pp. 5878–5884, 2019.

[10] O. Al-Ahmad, M. Ourak, J. Van Roosbroeck, J. Vlekken, and E. Vander Poorten, "Improved fbg-based shape sensing methods for vascular catheterization treatment," *IEEE Robotics and Automation Letters*, vol. 5, no. 3, pp. 4687–4694, 2020.

[11] J. P. Moore and M. D. Rogge, "Shape sensing using multi-core fiber optic cable and parametric curve solutions," *Optics express*, vol. 20, no. 3, pp. 2967–2973, 2012.

[12] X. T. Ha, D. Wu, M. Ourak, G. Borghesan, J. Dankelman, A. Menciassi, and E. Vander Poorten, "Shape sensing of flexible robots based on deep learning," *IEEE Transactions on Robotics*, vol. 39, no. 2, 2023.

[13] F. Khan, D. Barrera, S. Sales, and S. Misra, "Curvature, twist and pose measurements using fiber bragg gratings in multi-core fiber: A comparative study between helical and straight core fibers," *Sensors and Actuators A: Physical*, vol. 317, p. 112442, 2021.

[14] I. Floris, J. Madrigal, S. Sales, P. A. Calderón, and J. M. Adam, "Twisting measurement and compensation of optical shape sensor based on spun multicore fiber," *Mechanical Systems and Signal Processing*, vol. 140, p. 106700, 2020.

[15] S. Jäckle, V. García-Vázquez, T. Eixmann, F. Matysiak, F. von Haxthausen, M. M. Sieren, H. Schulz-Hildebrandt, G. Hüttmann, F. Ernst, M. Kleemann *et al.*, "Three-dimensional guidance including shape sensing of a stentgraft system for endovascular aneurysm repair," *International Journal of Computer Assisted Radiology and Surgery*, vol. 15, no. 6, pp. 1033–1042, 2020.

[16] X. T. Ha, M. Ourak, O. Al-Ahmad, D. Wu, G. Borghesan, A. Menciassi, and E. Vander Poorten, "Robust catheter tracking by fusing electromagnetic tracking, fiber bragg grating and sparse fluoroscopic images," *IEEE Sensors Journal*, vol. 21, no. 20, pp. 23 422–23 434, 2021.

[17] X. T. Ha, D. Wu, M. Ourak, G. Borghesan, A. Menciassi, and E. Vander Poorten, "Sensor fusion for shape reconstruction using electromagnetic tracking sensors and multi-core optical fiber," *IEEE Robotics and Automation Letters*, 2023.

[18] T. Vandebroek, M. Ourak, C. Gruijthuijsen, A. Javaux, J. Legrand, T. Vercauteren, S. Ourselin, J. Deprest, and E. Vander Poorten, "Macro-micro multi-arm robot for single-port access surgery," in *2019 IEEE/RSJ International Conference on Intelligent Robots and Systems (IROS)*. IEEE, 2019, pp. 425–432.

[19] T. F. Banchoff and S. T. Lovett, *Differential geometry of curves and surfaces*. AK Peters/CRC Press, 2010.

[20] B. K. Horn, "Closed-form solution of absolute orientation using unit quaternions," *Josa a*, vol. 4, no. 4, pp. 629–642, 1987.

[21] M. A. Diezinger, B. Tamadazte, and G. J. Laurent, "3d curvature-based tip load estimation for continuum robots," *IEEE Robotics and Automation Letters*, vol. 7, no. 4, pp. 10 526–10 533, 2022.

[22] F. Trauzettel, E. Vander Poorten, M. Ourak, J. Dankelman, and P. Breedveld, "3flex - 3d printable parametric tendon-driven manipulator," 2023.

[23] C. B. Barber, D. P. Dobkin, and H. Huhdanpaa, "The quickhull algorithm for convex hulls," *ACM Transactions on Mathematical Software (TOMS)*, vol. 22, no. 4, pp. 469–483, 1996.

[24] S. Jäckle, T. Eixmann, H. Schulz-Hildebrandt, G. Hüttmann, and T. Pätz, "Fiber optical shape sensing of flexible instruments for endovascular navigation," *International journal of computer assisted radiology and surgery*, vol. 14, pp. 2137–2145, 2019.

[25] M. Ourak, S. De Buck, X. T. Ha, O. Al-Ahmad, K. Bamps, J. Ector, and E. Vander Poorten, "Fusion of biplane fluoroscopy with fiber bragg grating for 3d catheter shape reconstruction," *IEEE Robotics and Automation Letters*, vol. 6, no. 4, pp. 6505–6512, 2021.

[26] Y. Ma, N. Gogin, P. Cathier, R. J. Housden, G. Gijsbers, M. Cooklin, M. O'Neill, J. Gill, C. A. Rinaldi, R. Razavi *et al.*, "Real-time x-ray fluoroscopy-based catheter detection and tracking for cardiac electrophysiology interventions," *Medical physics*, vol. 40, no. 7, p. 071902, 2013.